J. Physiol. (1979), **292**, *pp.* 149–166
With 12 *text-figures*
Printed in Great Britain

A QUANTITATIVE DESCRIPTION OF MEMBRANE CURRENTS IN RABBIT MYELINATED NERVE

BY S. Y. CHIU, J. M. RITCHIE, R. B. ROGART AND D. STAGG
From the Department of Pharmacology, Yale Univeristy School of Medicine, New Haven, Connecticut 06510, U.S.A.

(*Received 25 July 1978*)

SUMMARY

1. Voltage-clamp studies were carried out on single rabbit myelinated nerve fibres at 14 °C with the method of Dodge & Frankenhaeuser (1958).

2. A method was developed to allow the ionic currents through the nodal membrane to be calibrated exactly under voltage-clamp conditions by measuring the resistance of the internode through which the current was injected.

3. The ionic currents in a rabbit node of Ranvier can be resolved into two components, a sodium current and a leak current. Potassium current is almost entirely absent.

4. The sodium currents in rabbit nodes were fitted by the Hodgkin–Huxley model using m^2h kinetics. The kinetics of sodium currents in a rabbit node differ from that in a frog node under similar experimental conditions in two respects: (*a*) inactivation is faster, τ_h for rabbit being 2–3 times smaller around -50 mV; (*b*) the $P_{Na}(E)$ curve for mammal is shifted 10–15 mV in the hyperpolarizing direction.

5. From the kinetics of sodium current, the non-propagating rabbit action potential was reconstructed at 14 °C. The transient inward sodium current is responsible for the fast initial depolarization phase of the action potential, while the repolarizing phase is accounted for by leak alone. The computed shape of the action potential was in good agreement with the experimentally obtained action potential.

6. At 14 °C, frog and rabbit nodes with similar diameters have similar measured $\bar{g}_{Na}$ values.

INTRODUCTION

The ionic basis for nerve excitation was first elucidated in the squid giant axon by Hodgkin & Huxley (1952) who made the key observation that two separate, voltage-dependent, permeability changes underly the action potential: an early transient increase in permeability to sodium ions underlies the depolarization of the nerve membrane, and a delayed increase in permeability to potassium ions is largely responsible for repolarization. These permeability changes under voltage-clamp conditions were described by a set of empirical equations which were used to reconstruct the squid axon action potential. Subsequently, similar equations have been shown to apply to a variety of nerve fibres (Julian, Moore & Goldman, 1962; Dodge, 1961; Frankenhaeuser & Huxley, 1964; Goldman & Schauf, 1973; Shrager, 1974).

0022-3751/79/4030-0632 $01.50

The present study reports a detailed voltage-clamp analysis of the ionic currents in single rabbit myelinated nerve fibres. Mammalian fibres were first successfully voltage-clamped by Horackova, Nonner & Stämpfli (1968) and by Nonner & Stämpfli (1969). Although no detailed analysis was made, their results clearly showed the need for further study. For example, the potassium currents seemed to be entirely lacking. The present analysis shows that the currents in the rabbit node are indeed well described by the Hodgkin–Huxley formulation, except that voltage-dependent potassium currents are almost absent in these fibres (Horackova *et al.* 1968; Nonner & Stämpfli, 1969). Furthermore, the kinetics of sodium currents in rabbit nerve differ from those of frog in two ways: at the same temperature (14 °C), sodium currents in rabbit inactivate 2–3 times faster at about −50 mV than in frog; and the P_{Na} (E) curve in rabbit fibre is shifted 10–15 mV in the hyperpolarizing direction along the voltage axis when compared with the corresponding curve in the frog.

METHODS

The voltage-clamp studies were conducted by the method of Dodge & Frankenhaeuser (1958) as modified by Hille (1971*a*).

Rabbits of either sex, weighing about 5 kg, were killed by air injection into an ear vein. The sciatic nerves from both hind legs were removed, cleaned of fat, and desheathed. A side branch that seemed undamaged was gently pulled and a length of 2–4 cm cut from the main nerve bundle. This detached side branch was immersed in a pool of Locke solution and spread with two fine needles into a fan of interwoven fibres (see Stämpfli & Hille, 1976). A single fibre with three nodes visible was isolated by cutting away surrounding fibres leaving it attached at its two ends to the undissected portions of the trunk. It was transferred under Locke to a nerve chamber with four pools, *A*, *B*, *C*, *E*, separated by partitions (see Fig. 1). The node was positioned to lie in the *A* pool and Vaseline seals were applied to the surface of the three partitions. The fluid level was then lowered to expose the seals and remove conducting pathways between pools. The preparation was allowed to stabilize at 14 °C for 15–20 min before kinetic measurements were begun Single fibres from the frog *Rana pipiens* were similarly dissected and mounted. No effort was made to distinguish between motor and sensory fibres.

In the present experiments we assumed that for both frog and rabbit nodes the value of h_∞ is 0·75 at a holding potential of −80 mV (see Ulbricht & Wagner, 1975; Conti, Hille, Neumcke, Nonner & Stämpfli, 1976; Campbell & Hille, 1976). This procedure was adopted because of the uncertainties of the absolute membrane potential because of junction potentials. The junction potential, V_D, is intrinsically indeterminate; indeed, as Campbell & Hille (1976) point out 'in the node of Ranvier the potential V_D has never been measured'. In practice the setting of the holding potential control for $h_\infty = 0{\cdot}75$ was not significantly different for the two kinds of fibre, being $-86 \pm 1{\cdot}8$ mV ($n = 16$) for the frog node and $-84 \pm 2{\cdot}4$ mV ($n = 10$) for the mammalian node (which implies a junction potential of 4–6 mV). On two occasions, when we estimated the absolute membrane potential (at about $h_\infty = 0{\cdot}75$) from an estimate of the potential V_D inside the node made by measuring the values for resistors and determining directly the electrode and amplifier offset potentials, we obtained values of −80 and −84 mV for the absolute holding potential for two mammalian fibres and a value of −80 mV for one frog fibre. We believe, therefore, that the absolute holding potentials for the two types of fibres were similar.

The solution bathing the frog node was composed of (mM): NaCl, 115; $CaCl_2$, 2; KCl, 2·5; and morpholinopropane sulphonate (MOPS) buffer (pH 7·4), 10. Rabbit Locke solution contained (mM): NaCl, 154; $CaCl_2$, 2·2; KCl, 5·6; and MOPS buffer (pH 7·4), 10. In experiments involving TEA, NaCl was substituted by an equimolar amount of tetraethylammonium chloride (TEA-Cl). The ends of the nerve fibre were cut in 160 mM-KCl and 120 mM-KCl for rabbit and frog, respectively. Experiments were also done on fibres attached to the undissected nerve trunks.

Unless otherwise mentioned, potentials are reported as absolute membrane potential, E (inside minus outside).

All experiments were done at about 14 °C. Whenever possible the mean ± S.E. is given.

Resistance measurements and current calibration

In voltage-clamp experiments of myelinated nerves, the time course of the ionic currents is determined by measuring the voltage output of the voltage-clamp amplifier in the E-pool, V_E. The ionic current flowing into the nodal membrane is produced by applying a voltage across the internode ED, and is equal to V_E/R_{DE}. The value R_{DE} is usually estimated from geometrical

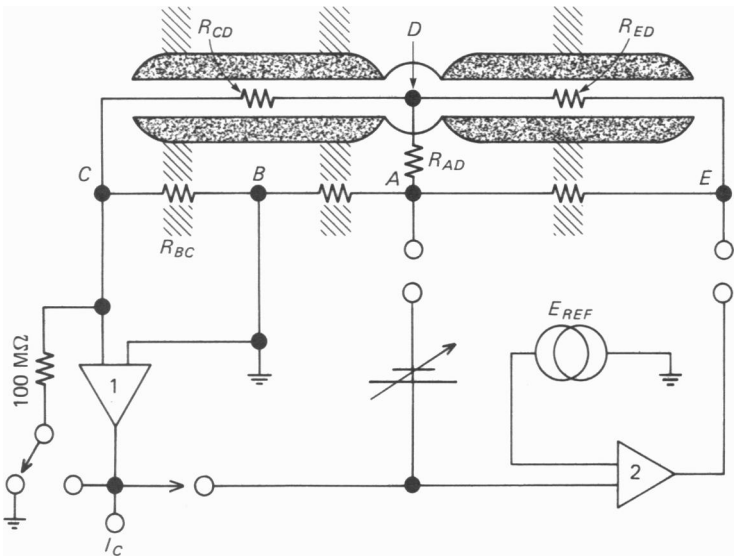

Fig. 1. Schematic representation of the voltage-clamp arrangement, illustrating a single myelinated nerve fibre lying over three insulating gaps separating four fluid-filled pools A, B, C and E. D represents the inside of the fibre at the node of Ranvier. The DC equivalent circuit for the fibre, with the four resistors R_{BC}, R_{CD}, R_{DE} and R_{AD}, is illustrated. R_{AD} represents the nodal membrane resistance. The amplifier output is ordinarily connected to the A-pool in the voltage-clamp arrangement, and is the membrane potential measuring amplifier. Also shown is the 100 MΩ feed-back resistor for measuring current in the C-pool (see Methods).

measurements and from assumed values of the resistivity of the internode. This involves uncertainties arising from inaccuracies in geometrical measurements of the internodes and from the unknown properties of the cut end of the fibre. In the present experiments, where $\bar{g}_{Na}$ values for rabbit and frog nerve fibres are compared, a series of measurements was devised to determine directly the internode resistances R_{DE}, R_{CD} and the resting nodal resistance, R_{AD}, for each fibre, as illustrated in Fig. 1.

To determine the three resistances, three independent measurements involving only these three quantities were made. Two of these measurements were: (1) current clamp measurement of the passive steady state voltage drop across the nodal membrane, V_{AD}, in response to a voltage applied to the E pool, V_E. This measurement involves the ratio of internodal resistance R_{DE} to nodal resistance R_{AD}; and (2) measurement of the current in the C pool, I_C, produced by a voltage V_E, applied between the E pool and the grounded A pool. At the end of the experiment the node of Ranvier was 'blown' with a sustained hyperpolarizing pulse to −350 mV. The final measurement was then made by: (3) application of a voltage to the A pool and measurement of

the current, I_C, in the C pool. This measurement involves only the resistance R_{CD}, since the nodal resistance, R_{AD}, is now close to zero. The three equations obtained are

$$R_{DE}/R_{AD} = \beta, \tag{1}$$

$$I_C = V_E.R_{AD}/(R_{CD}.R_{DE}+R_{DE}.R_{AD}+R_{CD}.R_{AD}), \tag{2}$$

$$I'_C = V_A/R_{CD}. \tag{3}$$

Since this method for measuring the resistances depends on 'blowing' the fibre, no corrections could be made for any changes in the internodal resistances during the experiment. However, on several occasions, R_{CD} was measured at various times up to 6 hr after the experiment and was found to be practically constant.

Data acquisition and analysis

Current and voltage recordings from the voltage-clamp were stored directly in a digital computer (Digital Equipment PDP 11/70). The analogue signal was low-pass filtered (4-pole Bessel characteristic filter, corner frequency 33 kHz) and then sampled with a high-speed sample-and-hold amplifier (Datel SHM5). Individual digital records consisting of 1000 readings at 12 μsec intervals were produced by a 12-bit analogue-to-digital converter (Datel EH12B3). The filter, sample-and-hold amplifier and analogue-to-digital converter were built into a special interface and the digital data were fed into the computer using direct memory access.

Computer programmes were developed in BASIC to perform leak subtraction, to extract kinetic parameters from sodium currents, and to find peak current values.

Three measurements were made to characterize the kinetics of the ionic currents in each fibre. First, the leak currents in response to hyperpolarizing steps, of 15, 30 and 45 mV were determined. Secondly, the current–voltage relation was obtained by measuring the ionic currents in response to a series of depolarizing pulses (increasing in steps of 7·5 mV) of 12 msec duration preceded by a 40 msec hyperpolarizing prepulse to -110 mV to remove resting inactivation. Finally, the $h_\infty(E)$ curve was measured with the standard procedure (see for instance Chiu, 1977).

Leak current subtraction

In principle the leak and capacitative currents could be subtracted from the total ionic current by scaling the current record obtained in response to a single hyperpolarizing step of 45 mV (from a holding potential of -80 mV) on the assumption that the leak current is proportional to the size of the voltage step. In practice, to reduce the effect of noise, the time course of the leak and capacitative currents associated with the -45 mV step was fitted by the equation:

$$I_L = F_0+F_1 \exp(-t/\tau_1)+F_2 \exp(-t/\tau_2),$$

which was then scaled to the individual records.

Peak current measurement

A programme was written to calculate the running average of each current record using a variable averaging width, typically 120 μsec. After the filtered record was compared visually with the original record, the absolute maximum or minimum of the filtered record was taken to be the peak inward or outward current.

Calculation of τ_m and τ_h

The sodium current at a given potential after leak subtraction was fitted by the equation:

$$I_{Na} = (1-\exp(-t/\tau_m))\, p(A \exp(-t/\tau_h)+B),$$

where A is an amplitude factor and B is the value of the current remaining at the end of a 12 msec test pulse because of incomplete sodium inactivation at small depolarizations. The values of A and τ_h were found from a least-squares fit of the logarithm of the decay portion of the sodium current (with the value of B subtracted) in the range 0·8–0·5 of the peak current value. The sodium current record was then divided point-by-point by the function $A \exp(-t/\tau_h)+B$. The result of this division was fitted by the function $(1-\exp\{(-t-\Delta t)/\tau\})^p$ using both $p = 2$ and $p = 3$. Δt was insignificant in comparison with τ_m and was ignored. Sodium currents

reconstructed from these calculated values of τ_h, τ_m, A and B were found to give a good fit to the experimentally observed currents with a value of $p = 2$ for rabbit and a value of $p = 3$ for the frog.

RESULTS

The action potential in a rabbit fibre

Fig. 2*A* shows a membrane action potential in a rabbit node at 14 °C in response to a rectangular pulse of current injected between *E* and *A* (Fig. 1). The action potential has a threshold of about 30 mV, lasts 3 msec, and reaches a height of 110 mV. For comparison, a frog action potential at 14 °C is shown in Fig. 2*B*; the duration, of about 3 msec, is similar to that calculated by Frankenhaeuser (1965) for toad node at 10 °C. It is apparent that at the same temperature, a rabbit and a frog action potential have similar shapes; the rabbit action potential, however, has a slightly faster upstroke and a slightly shorter duration.

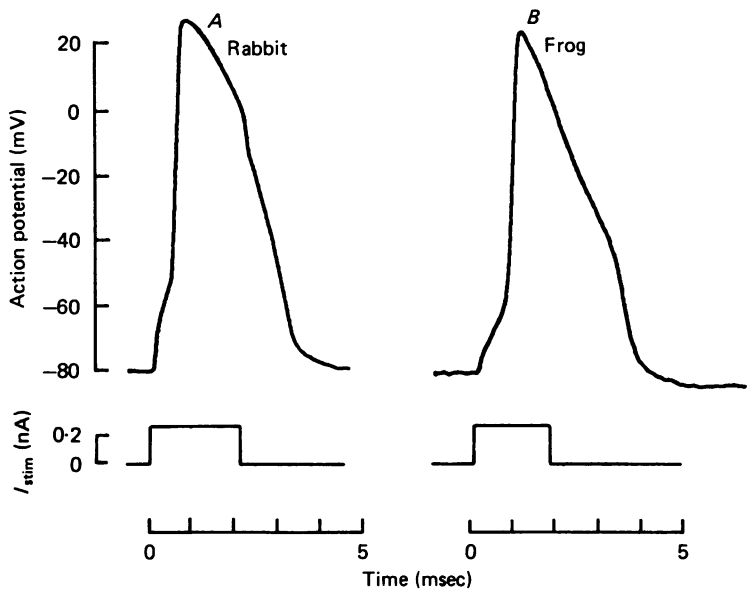

Fig. 2. Recorded membrane action potentials in a rabbit and a frog node of Ranvier. *A*, membrane action potential in a rabbit node and *B*, in a frog node at 14 °C. The shape of the stimulus current is shown below the action potential trace. Note the kink in the falling phase of the rabbit action potential corresponding to the termination of the stimulus current.

Ionic current in a rabbit node under voltage clamp

Under a maintained depolarization, the ionic current through the rabbit nodal membrane consists of an early inward current superimposed on an outward current (Fig. 3).

This early inward current, which is completely blocked by 500 nM-TTX (Fig. 3), becomes outward at about +15 mV to +50 mV (Table 1), shows kinetics similar to sodium currents in other excitable axons and has been assumed to be sodium current.

There was a large scatter in the individual values of E_{Na} (Table 1), which may indicate that rabbit fibres are more susceptible to stretch than frog fibres. It is interesting, however, that the average value of E_{Na} in the rabbit node was 27 mV, which is close to the theoretical value of 33 mV calculated on the basis of an intracellular sodium concentration of fresh cat nerve of 41 mM (Krnjević, 1955). The remaining outward current after treatment with 500 nM-TTX is characteristic of

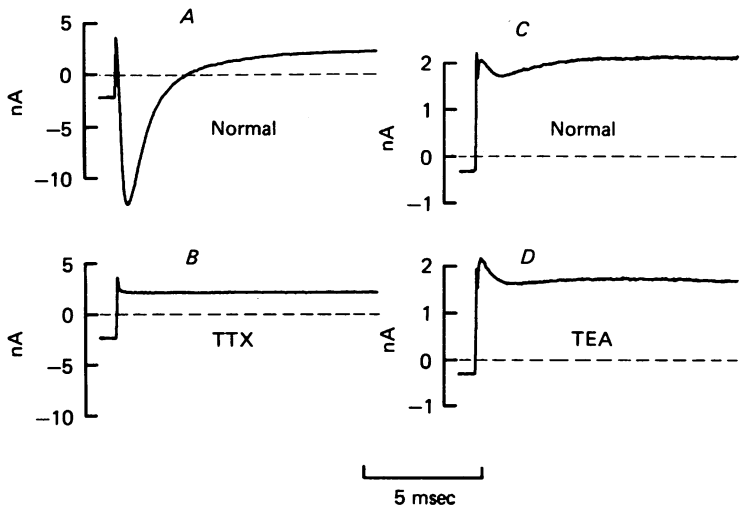

Fig. 3. Effect of TTX and TEA on the *total* ionic current in a rabbit node of Ranvier. *A*, the nodal membrane is hyperpolarized for 40 msec to −110 mV then depolarized to −35 mV. Only the last msec of the current trace corresponding to the hyperpolarizing prepulse is shown. Note the early inward current is superimposed on an outward current. *B*, complete blockade of the early current by 500 nM-TTX. *C*, the depolarization is to +60 mV. The early sodium current becomes outward and is superimposed on a huge outward current, which is almost insensitive to 17 mM-TEA-Cl, as shown in *D*. Temperature 14 °C.

passive leak. For example, its amplitude is linearly related to potential in the range −125–0 mV and it is not appreciably affected by TEA (Fig. 3*C* and *D*). In contrast, the ionic currents in a frog node after blocking all sodium currents with TTX show, besides a passive leak, a potential- and time-dependent rectifying late outward component, namely, the potassium current. In the rabbit node this latter current seems to be almost completely absent (Fig. 4), at least under the prssent experimental conditions, as seen also by Horackova *et al.* (1968) and Nonner & Stämpfli (1969).

The nodal ionic currents in rabbit can be written simply as: $I = I_{Na} + I_L$, with the usual notation. In the subsequent analysis, I_L was subtracted from the total current (see Methods). The resulting currents resemble those obtained from a frog node treated with TEA (Fig. 4*D*).

I–E relation for sodium current in a rabbit node of Ranvier

Fig. 5 shows the current–voltage relation for sodium current for a rabbit node at 14 °C (see Methods). The $\bar{g}_{Na}$ (E) relation, calculated by assuming an ohmic relation

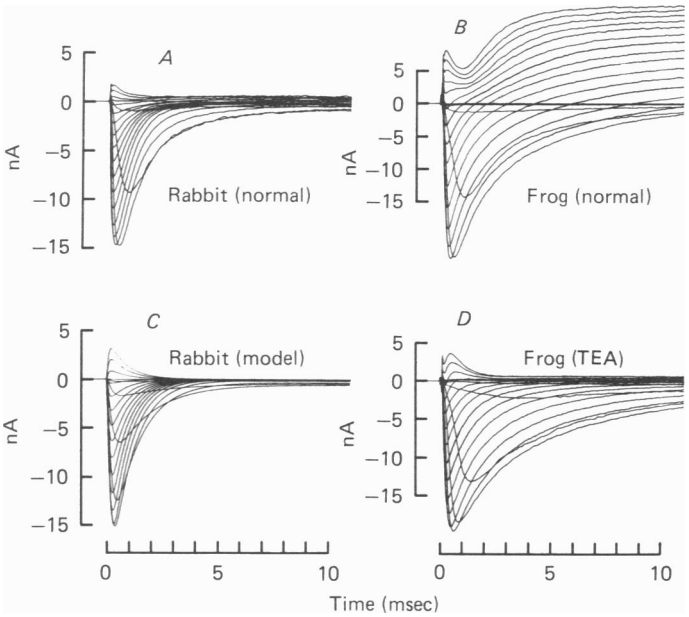

Fig. 4. Comparison of the ionic currents in rabbit and in frog nodes after leak subtraction at 14 °C. *A*, a family of ionic currents in a rabbit node generated by a series of equally spaced depolarization steps starting from the holding potential, −80 mV, and ending at +55 mV. *B*, the corresponding family of ionic currents in a frog node generated by a similar series of depolarizations. *C*, a family of sodium currents calculated on the basis of the Hodgkin–Huxley parameters for sodium current in rabbit node (Fig. 7, 10), with values of E_{Na} and $\bar{g}_{Na}$ from the fibre in *A*. *D*, addition of 12 mM-TEA-Cl to the Ringer bathing the frog node. Note that delayed rectification (potassium current) is present in the frog node but absent in the rabbit node. Ends of rabbit and frog fibres cut in 160 and 120 mM-KCl respectively. *B* and *D* are from two different frog fibres.

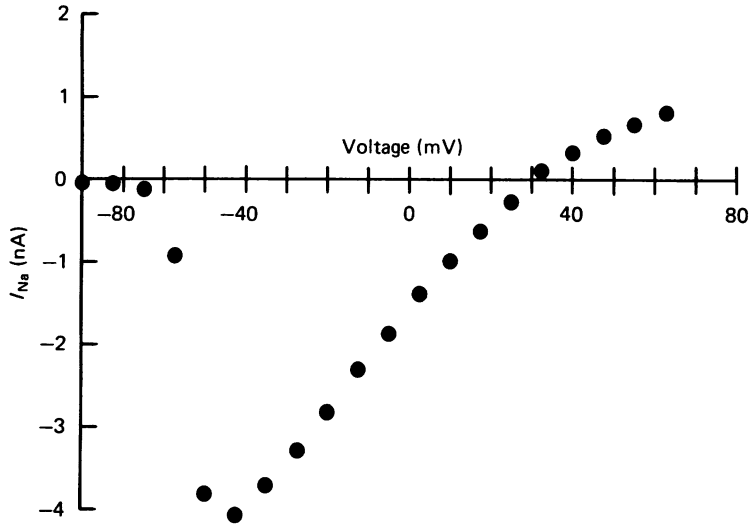

Fig. 5. Current–voltage relation for the sodium currents in a rabbit node. Ordinate: peak sodium current in nA. Abscissa: absolute membrane potential in mV. Temperature 14 °C.

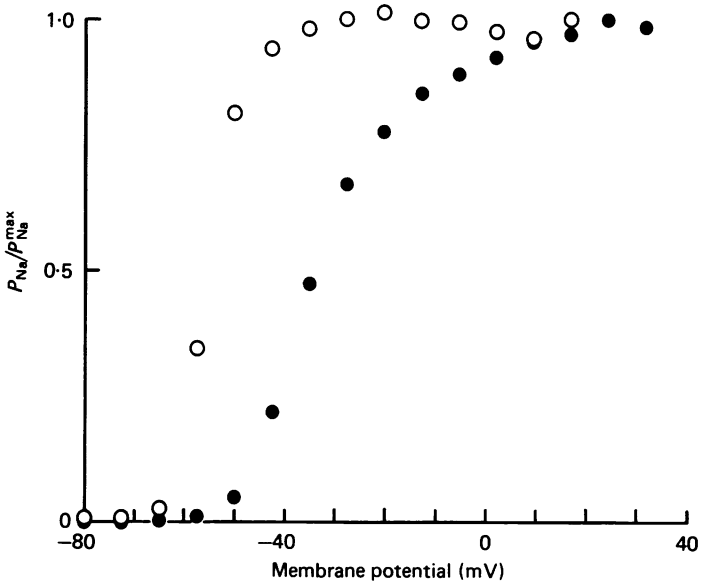

Fig. 6. Normalized $P_{Na}(E)$ relation for a rabbit node (○): a comparison with that of frog (●). The normalized $P_{Na}(E)$ relations for both fibres are calculated using the Goldman–Hodgkin–Katz constant field equation. Abscissa: absolute membrane potentials in mV. Ordinate: $P_{Na}(E)/P_{Na}^{max}(E_{max})$. The E_{max} values used to normalize the curves are −10 mV and +30 mV for rabbit and frog, respectively. Temperature 14 °C.

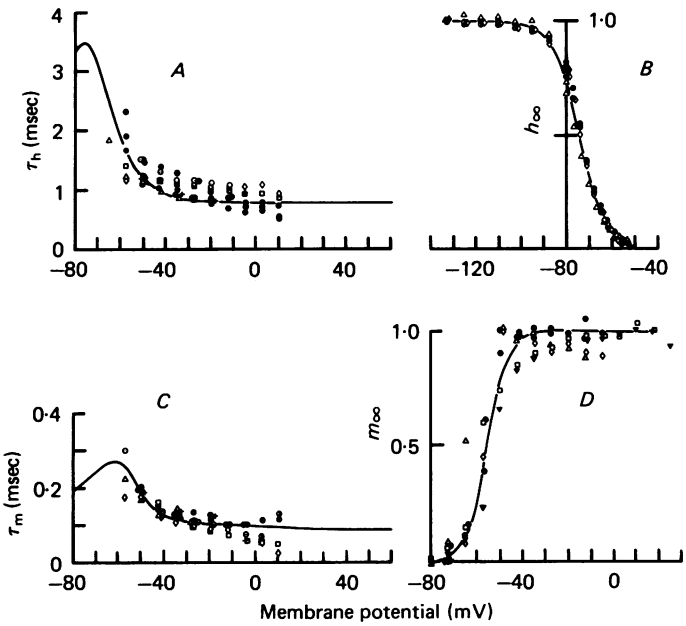

Fig. 7. Hodgkin–Huxley parameters for sodium currents in rabbit node at 14 °C. This Figure shows data from nine different rabbit fibres (◇, M8; ◐, M17; △, M19; +, M21; ⊕, M23; ◑, M25; ○, M29; □, M51; ▼, M52). *A*, $\tau_h(E)$; *B*, $h_\infty(E)$; *C*, $\tau_m(E)$; *D*, $m_\infty(E)$. The continuous lines in *B* and *D* are fitted to the experimental points and are of the form $(1+\exp(AE+B))^{-1}$ where *A* and *B* are constants. The continuous lines in *A* and *C* are derived from the fitted equations for β_h and α_m (in Fig. 10) together with the fitted equations for h_∞ and m_∞ (curves *B* and *D*). Note that this Figure and Fig. 9 contain results only from experiments designed to determine explicitly all the Hodgkin–Huxley kinetic parameters. They do not include experiments (such as some of those in Fig. 8) where the value of $\bar{g}_{Na}$ was determined simply by extrapolation (see legend to Fig. 8).

between sodium current and potential, showed a dip toward higher depolarizations. Thus, the Goldman–Hodgkin–Katz constant field equation (see Dodge & Frankenhaeuser, 1959) was used to calculate the peak permeabilities. Fig. 6 shows a typical normalized $P_{Na}(E)$ curve for a rabbit fibre (normalized with respect to the P_{Na} value at -10 mV). A corresponding normalized curve for $P_{Na}(E)$ for a frog fibre at the same temperature is shown for comparison. The two curves are clearly different: in the rabbit, the $P_{Na}(E)$ curve is shifted 10–15 mV in the hyperpolarizing direction along the potential axis (see also Fig. 9).

Kinetics of the sodium currents in a rabbit node

From the following equation for the sodium current

$$I_{Na} = \bar{P}_{Na}.m^2h.[Na]_0 (F^2 E/RT) (1-\exp\{(E-E_{Na}) F/RT\})/\{1-\exp(EF/RT)\}$$

the following parameters were determined by the standard methods (Hodgkin & Huxley, 1952; Frankenhaeuser, 1960): $\tau_h(E)$ (Fig. 7*A*), $h_\infty(E)$ (Fig. 7*B*), $\tau_m(E)$ (Fig. 7*C*), $m_\infty(E)$ (Fig. 7*D*) and $\bar{P}_{Na}$.

The values for $\bar{P}_{Na}$ were converted to conductance units at 0 mV by the following equation:

$$\bar{g}_{Na} = \bar{P}_{Na} F[Na]_0 \{\exp[(E-E_{Na}) F/RT]-1\}/(E-E_{Na})$$

When plotted against fibre diameter (Fig. 8), $\bar{g}_{Na}$ per node for rabbit fibre increases with fibre diameter. $\bar{g}_{Na}$ similarly depends on fibre diameter for frog node (Fig. 8). From Fig. 8, the average value for $\bar{g}_{Na}$ for rabbit node is $2{\cdot}2 \times 10^{-7} \pm 0{\cdot}6$ S (fibre diameter, $14{\cdot}4 \pm 1{\cdot}0$ μm, $n = 7$), whereas for frog node the average value for $\bar{g}_{Na}$ is $4{\cdot}4 \times 10^{-7} \pm 0{\cdot}5$ S (fibre diameter, $17{\cdot}5 \pm 0{\cdot}9$ μm, $n = 6$). Assuming that $\bar{g}_{Na}$ is linearly related to fibre diameter, the value of $\bar{g}_{Na}$ would be about the same in both rabbit and frog nodes of equivalent fibre diameter at 14 °C (i.e. the ratio $\bar{g}_{Na}$/fibre diameter, is $0{\cdot}15 \times 10^{-7}$ S μm^{-1} and $0{\cdot}25 \times 10^{-7}$ S μm^{-1} for rabbit and frog nodes respectively).

Comparison of the kinetics of sodium currents in rabbit and frog nodes

Similar procedures were used to measure the kinetic parameters for the frog node. Plots of the four parameters $\tau_m(E)$, $\tau_h(E)$, $h_\infty(E)$, $P_{Na}(E)/P_{Na}^{max}$ for the ten frog nodes of the present study are shown in Fig. 9. The continuous lines in this Figure are the values of these parameters calculated for the sodium currents in the rabbit node on the basis of a standard Hodgkin–Huxley model (with m^2h kinetics). A comparison of the sodium current kinetics in frog and rabbit nodes reveals the following features: $\tau_h(E)$ for rabbit was smaller than for frog, by a factor of 2–3 around -50 mV, and was less voltage-dependent over the potential range -50 to $+20$ mV. The value of $\tau_h(E)$ for frog varied much more from fibre to fibre than the corresponding value in the rabbit. However, the variability of $\tau_m(E)$ was about the same in both preparations.

Reconstruction of the action potential

The four rate constants for the sodium current (α_h, β_h, α_m, β_m) are derived from the values of $\tau_m(E)$, $\tau_h(E)$, $h_\infty(E)$ and $m_\infty(E)$ on the basis of the standard Hodgkin–Huxley equations (Hodgkin & Huxley, 1952).

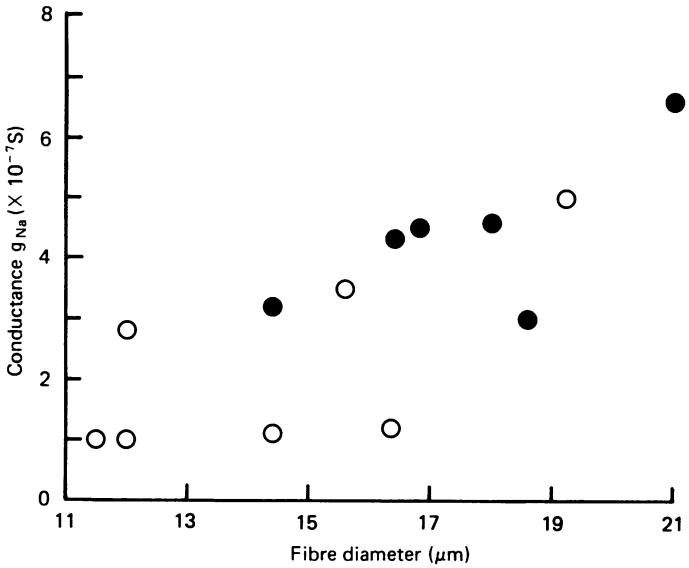

Fig. 8. The relationship between $\bar{g}_{Na}$ per node and fibre diameter in frog (●) and rabbit nodes (○). Ordinate: $\bar{g}_{Na}$ values in 10^{-7} S. Abscissa: fibre diameter in μm. Temperature 14 °C. Note that this Figure contains results from some experiments that were not included in Table 1 because they were too incomplete (both $\Delta E_m 1/2$ and ρ missing). In these experiments the calculations of $\bar{P}_{Na}$ (and hence $\bar{g}_{Na}$) were based on the value of the sodium current obtained by extrapolating its decay phase back to zero time (in a linear, least-squares, fit to a logarithmic plot of the decay phase between 85% and 45% of its peak value). This procedure assumed that the hyperpolarizing prepulse was large enough so that there was no initial inactivation (i.e. $h_0 = 1$) and that the depolarization was large enough so that $m_\infty = 1$.

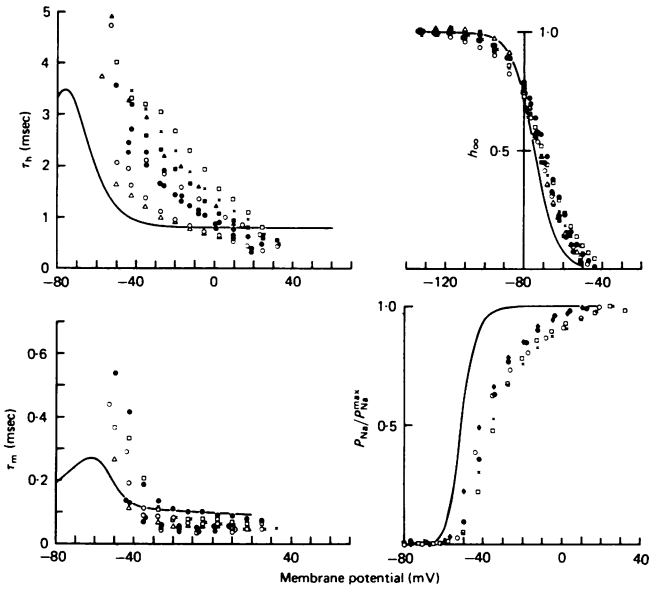

Fig. 9. Comparison of the kinetics of sodium currents in rabbit and frog nodes at 14 °C. The data for the $h_\infty(E)$, $\tau_m(E)$, $P_{Na}(E)$, P_{Na}^{max} and $\tau_h(E)$ plots have been obtained from ten different frog fibres. The continuous lines in this Figure represent the Hodgkin–Huxley parameters for the rabbit node at 14 °C (from Fig. 7). Note that $\tau_h(E)$ for frog is 2–3 times bigger than that of rabbit, around -50 mV, and that $m_\infty^2(E)$ for rabbit (from Fig. 7*D*) is shifted 10–15 mV in the hyperpolarizing direction, with respect to the $P_{Na}(E)$ curve of frog.

Since we did not study tail currents or use multiple pulse experiments to characterize τ_m and τ_h (and thus, α_h and β_m) over the hyperpolarizaing and low depolarizing potential range, we have chosen to fit only the β_h and α_m curves and use them together with the fitted curves for $m_\infty(E)$ and $h_\infty(E)$ to derive the corresponding values for $\alpha_h(E)$ and $\beta_m(E)$. Fig. 10 shows the values obtained for $\beta_h(E)$ and $\alpha_m(E)$ at 14 °C.

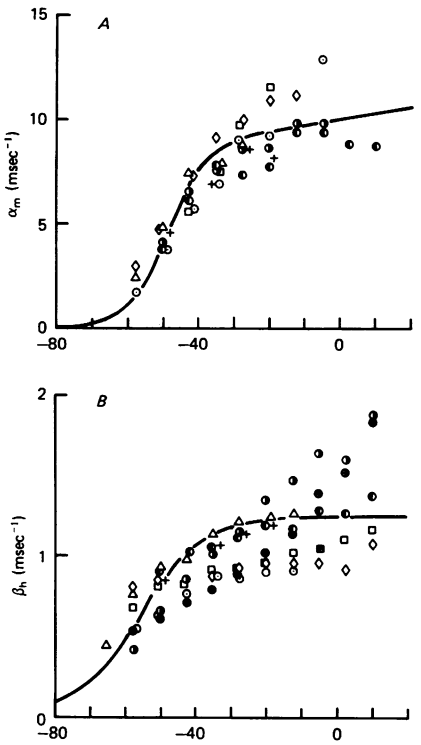

Fig. 10. Rate constants for sodium currents in rabbit node. Data are from eight different nodes. The continuous lines in *A* (α_m) and *B* (β_h) are calculated from the expressions

$$(0{\cdot}029E+10{\cdot}1)/(1+\exp[-0{\cdot}19(E+49)]) \quad \text{and} \quad 1{\cdot}25/(1+\exp[-0{\cdot}1(E+56)]),$$

respectively. These expressions are similar to those used by Frankenhaeuser & Huxley (1964). Note that the curves for α_m and β_h are extrapolated to somewhat more negative membrane potentials than those used experimentally.

The net membrane current, I_M, through a rabbit node can now be completely characterized as a function of time and voltage by the following equation:

$$I_M = I_{Na} + I_L + C\,dE/dt. \tag{4}$$

The passive nodal parameters for axon 17 (Table 1), together with a value of 2pF for the membrane capacitance determined in the same fibre from the measured membrane time constant, were used to calculate a non-propagating rabbit action potential to compare with the observed action potential obtained from the same axon as shown in Fig. 11. Except that it has a slightly smaller amplitude and a

TABLE 1. Measured nodal parameters for myelinated axons from rabbit: a comparison with those from frog. Temperature 14 °C

Axon	h_∞*	ΔE_m 1/2 (mV)	E_{Na} (mV)	$\bar{g}_{Na}$ ($\times 10^{-7}$ S)	$\bar{g}_L$ ($\times 10^{-7}$ S)	d (μm)	E_{ED} (MΩ)	R_{OD} (MΩ)	l_{FD} (cm)	l_{OD} (cm)	ρ (Ω.cm)
					Frog						
F 2	0·79	41	45	4·6	0·32	18·0	12	—	0·12	—	124
F 6	0·78	33	45	1·5	0·23	—	30	17	—	—	—
F 8	0·84	38	44	6·6	0·85	21·0	6	15	0·05	0·14	193
F 10	0·75	48	46	3·0	0·26	18·6	10	8	0·14	0·12	92
F 12	0·72	45	46	3·2	0·34	14·4	14	25	0·08	0·11	161
F 14	0·77	35	31	4·3	0·56	16·4	19	21	—	—	—
F 16	0·75	35	33	2·0	0·25	—	31	29	—	—	—
F 18	0·74	48	45	2·4	0·14	—	23	67	0·05	0·12	—
F 19	0·72	40	47	4·5	0·34	16·8	13	26	0·07	0·12	218
F 57	0·75	40	—	—	—	—	—	—	—	—	—
F 74	0·75	45	—	—	—	—	—	—	—	—	—
F 87	0·79	41	—	—	—	—	—	—	—	—	—
F 91	0·79	46	—	—	—	—	—	—	—	—	—
					Rabbit						
M 8	0·76	25	25	—	—	—	—	—	—	—	—
M 17	0·77	26	51	1·1	0·11	14·4	89	89	—	—	—
M 19	0·74	20	15	—	—	—	—	—	—	—	—
M 21	0·86	20	16	2·8	0·68	12·0	33	—	—	0·12	152
M 24	—	—	—	—	—	16·3	17	16	0·06	0·15	199
M 25	0·80	25	31	1·0	0·10	11·5	106	60	—	0·13	234
M 29	0·65	20	12	1·0	0·21	12·0	103	31	—	—	—
M 40	—	—	—	—	—	15·6	14	16	0·12	—	109
M 50	—	—	—	5·0	0·46	19·2	25	20	0·14	0·14	228
M 51	0·70	25	40	—	—	—	—	—	—	—	—
M 52	0·72	30	29	—	—	16·0	9.3	15·5	0·09	0·14	105

					Mean ± S.E.						
Rabbit	0·75	24	27	2·2	0·31	14·6	50	35	0·11	0·14	171
	± 0·02	± 1·3	± 5	± 0·8	± 0·11	± 0·9	± 15	± 11	± 0·02	± 0·01	± 23
Frog	0·76	41	43	3·6	0·37	17·5	18	26	0·09	0·12	158
	± 0·01	± 1·4	± 1·6	± 0·5	± 0·07	± 0·9	± 3	± 6	± 0·02	0·00	23

* Note that the holding potential in both frog and rabbit experiments was adjusted to give a value of h_∞ for each fibre of about 0·75.

h_∞ = value of h_∞ at the holding potential.

$\Delta E_m\ 1/2 = E_m\ 1/2 - E_H$ (where $E_m\ 1/2$ is the mid-point potential for the $P_{Na}(E)$ curve, E_H is the holding potential).

E_{Na} = reversal potential for sodium current (mV).

$\bar{g}_{Na}$ = maximum sodium conductance for whole node ($\times 10^{-7}$ S).

$\bar{g}_L$ = leak conductance for whole node ($\times 10^{-7}$ S).

d = fibre diameter, usually measured in B-pool after experiment.

R_{DE}, R_{CD} = internodal resistances in MΩ (see Fig. 1).

l_{DE}, l_{CD} = respective internodal lengths in cm.

ρ = effective resistivity of the internode calculated from our data using the equation:

$$\rho = \left(\frac{\pi d_o^2 R_{DE}}{4 l_{DE}} + \frac{\pi d_o^2 R_{CD}}{4 l_{CD}}\right) 12,$$

where d_0 (axon diameter) = $0{\cdot}7 \times d$ (fibre diameter). The method developed in this paper to measure the internodal resistances gives an effective value for ρ of 158 ± 23 Ωcm for frog fibres as compared to the value of 114 Ωcm obtained by Tasaki (see Stämpfli & Hille, 1976).

broader duration, the computed action potential is essentially similar to the observed potential at 14 °C.

Fig. 12 illustrates the computed ionic currents underlying a rabbit action potential and the similar currents computed for frog, using our own kinetics for frog sodium current and using those for potassium currents taken from Hille (1971*b*).

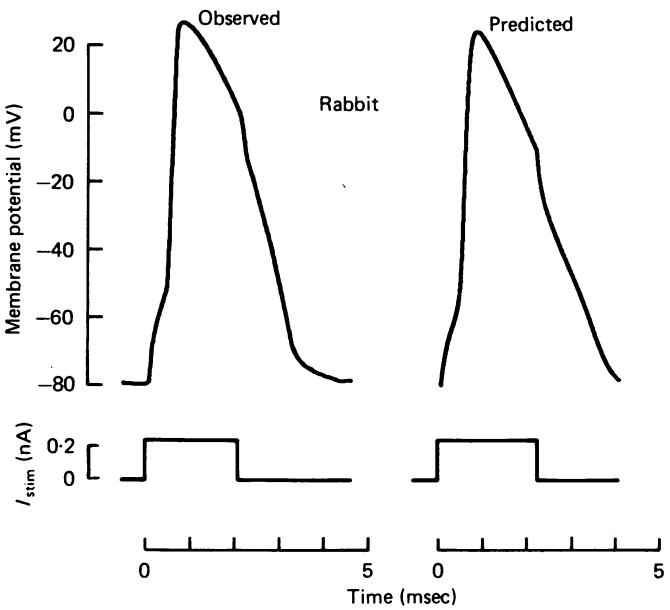

Fig. 11. Reconstruction of a rabbit membrane action potential at 14 °C. The action potential on the left is recorded from axon M17 (also represented by ◐ in Figs. 7 and 10). The action potential on the right is calculated by integrating eqn. (4) (see p. 159) numerically over time with the initial conditions that $E(t = 0) = -80$ mV and $I_M = 0{\cdot}25$ nA for $0 < t < 2{\cdot}1$ msec, $I_M = 0$ for $t \geqslant 2{\cdot}1$ msec. The effect of the prolonged stimulus is shown by the kink in the falling phase of the calculated potential. Note that the calculation of the tail end of the action potential is based on the extrapolated portions of the α_m and β_h curves in Fig. 10.

Comparison of the time courses of ionic currents underlying the frog and rabbit action potential at 14 °C reveals the following features: (*a*) The outward current responsible for repolarization in rabbit is entirely leak, whereas in frog, it is leak plus potassium current, (*b*) the computed time course of I_{Na} for a frog fibre has two peaks (see Fig. 8, Hodgkin & Huxley, 1952; Frankenhaueser & Huxley, 1964), the first one occurring at the peak of the action potential and the second one occurring during activation of the late potassium current; this is in contrast to the existence of only the initial hump in the computed time course of I_{Na} underlying a rabbit action potential.

DISCUSSION

One purpose of this investigation has been to examine quantitatively the applicability of the ionic hypothesis of Hodgkin & Huxley (1952) to excitation in the rabbit myelinated fibre. Our results show that, as in squid and frog nerve, a transient

inward sodium current is responsible for the initial fast depolarization during the rabbit action potential. However, unlike that in squid and frog nerve, the outward current responsible for repolarizing the membrane in rabbit nerve at 14 °C consists of only one ionic component, the passive leak: potassium currents are virtually absent. A family of voltage-clamp current records for a rat node at 37 °C published by Nonner & Stämpfli (1969) also shows the absence of potassium current (see also

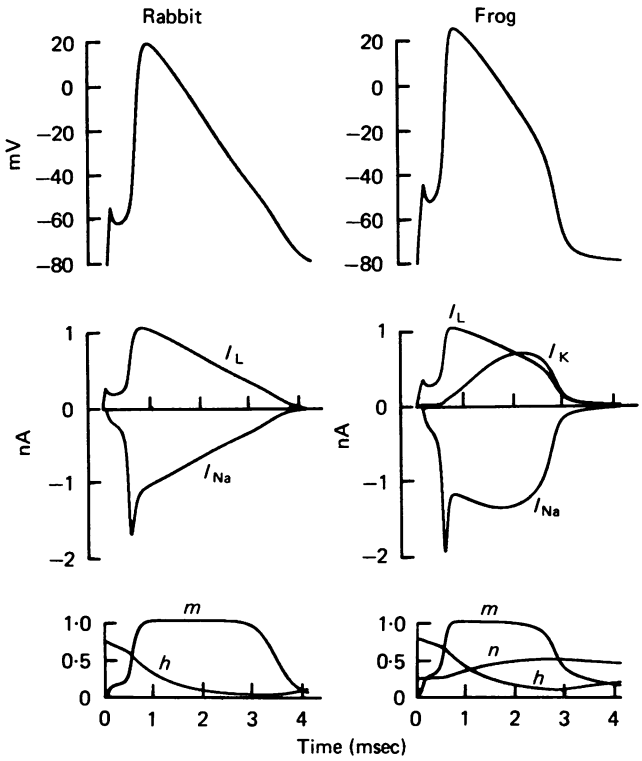

Fig. 12. Comparison of the computed time courses of the ionic currents underlying rabbit and frog action potential at 14 °C. Note the existence of two peaks in the time course of I_{Na} during the frog membrane action potential and the existence of only the initial peak for I_{Na} in the rabbit. Note also that the repolarizing current is leak plus potassium current in the frog whereas it is only leak current in the rabbit node. Temperature 14 °C.

Burg, 1970). Three possibilities could account for our failure to detect potassium currents in the rabbit fibre: damage to the nerve fibre during dissection; a lack of Hodgkin–Huxley type potassium channels; or shifted voltage-dependent kinetics for potassium channels. The first possibility seems unlikely, since even our best fibres (which had a small leak current, a large sodium current and a sodium reversal potential of +20 to +50 mV) show little or no potassium current. Unfortunately, our present experiments cannot distinguish between the remaining alternatives, namely that of shifted voltage-dependent kinetics of existing potassium channels so that they are never activated over the voltage range or at the temperature (14 °C) used experimentally, and the alternative of complete lack of potassium channels.

Despite the lack of potassium currents, the rabbit action potential at 14 °C has a duration similar to that of the frog (Fig. 2). The reason for this is that the sodium currents in the rabbit node inactivates 2–3 times faster than those in the frog node. The value of $\bar{g}_L$ in rabbit is about the same as in the frog (Table 1). Thus, potassium currents are unnecessary in repolarizing a rabbit nodal membrane. The relative roles played by leak and potassium currents in repolarizing the membrane clearly varies among different types of axons. In the squid, the potassium current plays an important role in repolarization, as revealed by the low $\bar{g}_L/\bar{g}_K$ ratio of 0·008 (Hodgkin & Huxley, 1952), and by the experimental observation that blocking the potassium current with TEA significantly prolongs the action potential (Armstrong, 1966). In the frog node, where $\bar{g}_L/\bar{g}_K$ is 0·19 (Hille, 1971*b*), i.e. about 30 times higher than in squid, the potassium current plays only a secondary role in repolarization: TEA treatment in frog nerves seldom lengthens the action potential by more than 50 %, motor nerves being affected more than sensory nerves (Stämpfli & Hille, 1976). Furthermore, in experiments with extracellular recording from single myelinated fibres in the rat ventral roots, Bostock, Sherratt & Sears (1978) have recently shown that TEA is quite ineffective, even in concentrations as high as 60 mM, in prolonging the action potential.

The observation that the P_{Na} (E) curve in rabbit is shifted 10–15 mV in the hyperpolarizing direction along the voltage axis relative to that of frog (when their h_∞ curves are superimposed) is interesting in the light of a similar shift reported by Adrian & Marshall (1977) for mammalian muscle compared with amphibian skeletal muscle. The negative shift of 10–15 mV described here may reflect either a difference in the kinetics of the sodium current or a difference in the nodal series resistance. An increased series resistance will shift the m_∞ (E) curve in the hyperpolarizing direction and make it steeper (Chandler & Meves, 1970): to produce a shift of 10–15 mV, a series resistance of 1–2 MΩ would be required. This would have predictable consequences on the performance of the clamp around threshold potential. For example, a stable sodium current would be difficult to obtain when the depolarization is around threshold, which is -50 to -60 mV and corresponds to the mid-point potential of the m_∞ (E) curve (Fig. 7*D*). However, in 'good' experiments we obtained reasonably stable sodium currents around the mid-point potential of the m_∞ (E) curve (stable in the sense that successive tests gave similar currents). More experiments should be done to determine the effect of a series resistance on the measurable kinetics of sodium channel in the rabbit by decreasing inward current strengths either by TTX or lowering the external sodium concentration.

The exact value of the resting potential in these fibres is slightly uncertain (see Methods); and it has been assumed in this paper that the value of h_∞ is 0·75 at a membrane potential of -80 mV in order to compare the kinetic properties of the rabbit and frog fibres. This, however, would not differentially affect the analysis of the results for rabbit and frog fibres. Thus, in the rabbit the mid-point of the P_{Na} (E) curve is 24 mV more positive than the potential at which $h_\infty = 0{\cdot}75$, whereas it is 41 mV more positive in the frog (Table 1). This difference, which is highly significant statistically, is independent of any assumption on the exact placing of the h_∞ curve.

It is interesting to note that Ritchie (1978) found that the maximum binding capacity of saxitoxin to myelinated nerve is 5 times higher in rabbit than that in

frog nodes. However, the present voltage-clamp data (at 14 °C) do not seem to support a fivefold difference in sodium channel density of rabbit and frog nodes: for $\bar{g}_{Na}$ is comparable in both types of fibre of equivalent diameter (Fig. 8). This discrepancy remains to be resolved.

We wish to thank Dr Fred Sigworth for his valuable advice throughout the investigation and particularly for suggesting a method for measuring the fibre resistance. This work was supported by a grant NS-12327 from the U.S.P.H.S. and by a grant RG 1162 from the National Multiple Sclerosis Society.

REFERENCES

ARMSTRONG, C. M. (1966). Time course of TEA^+-induced anomalous rectification in squid giant axons. *J. gen. Physiol.* **50**, 491–503.

ADRIAN, R. H. & MARSHALL, M. W. (1977). Sodium currents in mammalian muscle. *J. Physiol.* **268**, 223–250.

BOSTOCK, H., SHERRATT, R. M. & SEARS, T. A. (1978). Overcoming conduction failure in demyelinated nerve fibres by prolonging action potentials. *Nature, Lond.* **274**, 385–387.

BURG, D. (1970). Untersuchungen am Ranvierschen Schnürring einzelner Taubennervenfasern. *Pflügers Arch. ges. Physiol.* **317**, 278–286.

CAMPBELL, D. & HILLE, B. (1976). Kinetic and pharmacological properties of the sodium channel of frog skeletal muscle. *J. gen. Physiol.* **67**, 309–323.

CHANDLER, W. K. & MEVES, H. (1970). Rate constants associated with changes in sodium conductance in axons perfused with sodium fluoride. *J. Physiol.* **211**, 679–705.

CHIU, S. Y. (1977). Inactivation of sodium channels: second order kinetics in myelinated nerve. *J. Physiol.* **273**, 573–596.

CONTI, F., HILLE, B., NEUMCKE, B., NONNER, W. & STÄMPFLI, R. (1976). Measurement of the conductance of the sodium channel from current fluctuations at the node of Ranvier. *J. Physiol.* **262**, 699–727.

DODGE, F. A. (1961). Ionic permeability changes underlying nerve excitation. In *Biophysics of Physiological and Pharmacological Actions*. Washington: AAAS.

DODGE, F. A. & FRANKENHAEUSER, B. (1958). Membrane currents in isolated frog nerve fibre under voltage clamp conditions. *J. Physiol.* **143**, 76–90.

DODGE, F. A. & FRANKENHAEUSER, R. (1959). Sodium currents in the myelinated nerve fibre of *Xenopus laevis* investigated with the voltage clamp technique. *J. Physiol.* **148**, 188–200.

FRANKENHAEUSER, B. (1960). Quantitative description of sodium currents in myelinated nerve fibres of *Xenopus laevis*. *J. Physiol.* **151**, 491–501.

FRANKENHAEUSER, B. (1965). Computed action potential in nerve from *Xenopus laevis*. *J. Physiol.* **180**, 780–787.

FRANKENHAEUSER, B. & HUXLEY, A. F. (1964). The action potential in the myelinated nerve of *Xenopus laevis* as computed on the basis of voltage clamp data. *J. Physiol.* **171**, 302–315.

GOLDMAN, L. & SCHAUF, C. L. (1973). Quantitative description of sodium and potassium currents and computed action potentials in *Myxicola* giant axons. *J. gen. Physiol.* **61**, 361–384.

HILLE, B. (1971*a*). The permeability of the sodium channel to organic cations in myelinated nerve. *J. gen. Physiol.* **58**, 599–619.

HILLE, B. (1971*b*). Voltage clamp studies on myelinated nerve fibres. In *Biophysics and Physiology of Excitable Membranes*, ed. ADELMAN, W. J., pp. 230–246. New York: Van Nostrand Reinhold.

HODGKIN, A. L. & HUXLEY, A. F. (1952). A quantitative description of membrane current and its application to conduction and excitation in nerve. *J. Physiol.* **117**, 500–544.

HORACKOVA, M., NONNER, W. & STÄMPFLI, R. (1968). Action potentials and voltage clamp currents of single rat Ranvier nodes. *Proc. int. Union Physiol. Sci.* **7**, 198.

JULIAN, F. J., MOORE, J. W. & GOLDMAN, D. E. (1962). Current-voltage relations in the lobster giant axon membrane under voltage clamp conditions. *J. gen. Physiol.* **45**, 1217–1238.

KRNJEVIĆ, K. (1955). The distribution of Na and K in cat nerve. *J. Physiol.* **128**, 473–488.

NONNER, W. & STÄMPFLI, R. (1969). A new voltage clamp method. In *Laboratory Techniques in Membrane Biophysics*, ed. PASSOW, H. & STÄMPFLI, R. Berlin: Springer-Verlag.

RITCHIE, J. M. (1978). Sodium channel as a drug receptor. In *Cell Membrane Receptors for Drugs and Hormones – A Multidisciplinary Approach*, ed. STRAUB, R. W. & BOLIS, L., pp. 227–242. New York: Raven.

SHRAGER, P. (1974). Ionic conductance changes in voltage clamped crayfish axons at low pH. *J. gen. Physiol.* **64**, 666–690.

STÄMPFLI, R. & HILLE, (1976). Electrophysiology of the peripheral myelinated nerve. In *Frog Neurobiology*, ed. LLINAS, R. & PRECHT, W. Berlin: Springer-Verlag.

ULBRICHT, W. & WAGNER, H.-H. (1975). The influence of pH on equilibrium effects of tetrodotoxin on myelinated nerve fibres of *Rana esculenta*. *J. Physiol.* **252**, 159–184.